NEOPLASIA
www.neoplasia.com

Volume 18 Number 2 February 2016 pp. 82–89 82

Evaluation of Concurrent Radiation, Temozolomide and ABT-888 Treatment Followed by Maintenance Therapy with Temozolomide and ABT-888 in a Genetically Engineered Glioblastoma Mouse Model

Benjamin Lemasson*, Hanxiao Wang†, Stefanie Galbán‡, Yinghua Li#, Yuan Zhu#, Kevin A. Heist†, Christina Tsein§, Thomas L. Chenevert†, Alnawaz Rehemtulla§, Craig J. Galbán†, Eric C. Holland¶ and Brian D. Ross†

*University Joseph Fourier, Grenoble Institut des Neurosciences, Grenoble, France; †Department of Radiology, University of Michigan, Ann Arbor, MI, 48109 USA; ‡Department of Pathology, University of Michigan, Ann Arbor, MI, 48109 USA; §Department of Radiation Oncology, University of Michigan, Ann Arbor, MI, 48109 USA; ¶Department of Neurological Surgery, Fred Hutchinson Cancer Research Center, University of Washington, Seattle, WA 98109 USA; #Children's Research Institute, NW Washington, DC 20010, USA. Department of Radiation Oncology, Washington University, St. Louis, MO 63110, USA

Abstract

Despite the use of ionizing radiation (IR) and temozolomide (TMZ), outcome for glioblastoma (GBM) patients remains dismal. Poly (ADP-ribose) polymerase (PARP) is important in repair pathways for IR-induced DNA damage and TMZ-induced alkylation at N7-methylguanine and N3-methyldenine. However, optimized protocols for administration of PARP inhibitors have not been delineated. In this study, the PARP inhibitor ABT-888 was evaluated in combination with and compared to current standard-of-care in a genetically engineered mouse GBM model. Results demonstrated that concomitant TMZ/IR/ABT-888 with adjuvant TMZ/ABT-888 was more effective in inducing apoptosis and reducing proliferation with significant tumor growth delay and improved overall survival over concomitant TMZ/IR with adjuvant TMZ. Diffusion-weighted MRI, an early translatable response biomarker detected changes in tumors reflecting response at 1 day post TMZ/IR/ABT-888 treatment. This study provides strong scientific rationale for the development of an optimized dosing regimen for a PARP inhibitor with TMZ/IR for upfront treatment of GBM.

Neoplasia (2016) 18, 82–89

Introduction

Glioblastoma (GBM) is the most common and aggressive of malignant primary brain tumor in adults [1]. Standard-of-care for newly diagnosed GBM patients includes surgery, irradiation (IR) with both concurrent and adjuvant temozolomide (TMZ) however the median survival time for GBM patients is only about 15 months and the 5-year survival rate is less than 10% [2]. Defects in DNA repair pathways are known to limit the efficacy of anticancer therapies [3,4] thus this study was undertaken to evaluate the effects of the poly(ADP-ribose) polymerase (PARP) inhibitor ABT-888 (Veliparib) for GBM treatment.

Address all correspondence to: Brian D. Ross, Ph.D., University of Michigan, Center for Molecular Imaging, Biomedical Sciences Research Building, 109 Zina Pitcher Place, Ann Arbor, MI 48109–2200.
E-mail: bdross@umich.edu
Received 14 September 2015; Revised 17 November 2015; Accepted 23 November 2015

1476-5586
http://dx.doi.org/10.1016/j.neo.2015.11.014

PARPs are a large family of enzymes with essential roles in DNA repair, which can render cancer cells resistant to DNA damaging agents [5]. A number of PARP inhibitors have been or are currently in development pre-clinically [6] and clinically (NCT00770471, NCT01514201) [7,8]. When used alone, PARP inhibitors show high potency in tumors where DNA repair capacity is impaired, such as deficiency in BRCA genes. Olaparib, a PARP inhibitor, was recently approved to treat ovarian cancer patients who have BRCA1 and BRCA2 mutations and failed three or more chemotherapy treatments [9]. Meanwhile, PARP inhibitors used in combination with DNA damaging interventions achieved optimal therapeutic results [10].

Concurrent TMZ/IR followed by adjuvant TMZ is standard-of-care for GBM patients, thus the addition of a PARP inhibitor may provide a therapeutic benefit. ABT-888 is a potent PARP inhibitor targeting both PARP-1 and PARP-2, is orally bioavailable and demonstrates blood–brain barrier penetration [11,12]. ABT-888 has been evaluated in combination with chemotherapies and/or radiation therapy in several preclinical studies and early stage clinical trials [13–17].

Assessment and quantification of orthotopic tumor volumes and growth rates in response to therapy was done using MRI which allowed for non-invasive assessment of tumors over time. In addition, diffusion-weighted MRI (DW-MRI) allowed for obtaining information related to the microscopic cellular environment of solid tumors [18]. Since water diffusion values have been shown to be affected by changes in cellular density, DW-MRI can be consider a surrogate imaging biomarker for characterizing treatment effects [19].

In this study, a primary GBM genetically engineered mouse model [20] was used to evaluate if significant therapeutic benefit could be achieved by the addition of a PARP inhibitor (ABT-888) to TMZ/IR therapy. MRI was used to quantify and serially follow therapeutic-associated changes in brain tumor volumes and cellularity during treatment for the dosage groups under evaluation. Overall, results revealed that inclusion of ABT-888 as part of standard of care therapy significantly improved the overall outcome of treated mice and supports clinical evaluation in this context.

Material and Methods

Mouse Glioma Model

A genetically engineered GBM mouse model that recapitulates defects in the key signaling pathways in GBM, where PDGF is overexpressed and PTEN is deleted in nestin expressing cells in an ink4/arf deficient background was used for these studies [21–25]. In brief, Ntv-a mice were injected i.c. with 10^4 DF-1 cells transfected with RCAS-PDGF retroviral vectors within 24 hours post-gestation. The RCAS/tv-a system generated PDGF-B driven gliomas in *nestin-t-va/ink4a-arf−/−/pten*$^{fl/fl}$ mice which developed tumors with a 90% to 95% incidence, resulting in the formation of high-grade gliomas within 4 to 6 weeks post-injection. The model is an attractive GBM model as tumors share high-grade elements such as microvascular proliferation, pseudopalisading necrosis and leaky vasculature with human GBMs [24]. These tumors also closely mimic the proneural subtype of GBM, in which *CDKN2A* (encoding for both *p16INK4A* and *p14ARF*) and *PTEN* deletion are observed in up to 56% and 69% proneural human gliomas, respectively [26]. In order to dissect the role of ABT-888 in the sensitivity of gliomas to TMZ and IR, we utilized PDGF-B driven PTEN-deficient and PTEN-intact gliomas. Mice were monitored daily for symptoms of tumor development and at 4 weeks of age, mice were screened for tumors using MRI.

Treatment Protocol

Animals were randomized into treatment groups when MRI-determined tumor volumes reached 20-30mm^3 as measured by multi-slice MRI. To investigate the efficacies of various combination and individual therapies, tumor-bearing animals were divided into eight groups and treated with vehicle (1% DMSO in saline, n = 9), ABT-888 (25 mg/kg per dose, 2 doses a day, 5 d/wk for 2 weeks, n = 12), TMZ (50mg/kg/day, 5 days/week for 2 weeks, n = 8), IR (1 Gy/d, 5 d/wk for 2 weeks, n = 13), TMZ/ABT-888 (2 weeks of TMZ/ABT-888 treatment, n = 8), IR/ABT-888 (2 weeks of ABT-888/IR treatment, n = 9), TMZ/IR (2 weeks of IR/TMZ treatment followed by 2 weeks of TMZ treatment, n = 5), and TMZ/IR/ABT-888 (2 weeks of IR/TMZ treatment followed by 2 weeks of TMZ/ABT-888 treatment, n = 6) as shown in Figure 1. Animal care procedures were approved by the University Committee on Use and Care of Animals (UCUCA). In late stages of tumor growth, mice may develop lethargy, weight loss and loss in coordination. If these symptoms become severe, the animals were euthanized according to approved UCUCA End Stage Illness Policy and the Tumor Scoring Guidelines.

Ionizing radiation of mice was accomplished at 320 kVp and 10 mA using an IC-320 orthovoltage irradiator (Kimtron Medical, Bantam, CT). A 6 × 8 cm cone was used at a source-to-surface distance of 40 cm at a dose rate of ~138 cGy/min. To ensure proper calibration of the delivered dose, dosimetry was accomplished using an ionization chamber connected to an electrometer system that was directly traceable to a National Institute of Standards and Technology calibration. Mice were positioned and the whole brain was irradiated while the rest of the body was shielded using a lead secondary collimator. *In vivo* administration of compounds along with radiation therapy (IR; 1 Gy/day) were administered concurrently daily for 5 days a week over the initial 2-week period.

In order to quantify treatment effects in dosage groups, survival and progression-free survival times were used as endpoints along with time-to-progression. Survival was assessed by mice at the time of reaching the End Stage Illness criteria as outline above. Progression of mice was determined as the time the tumor volume progressed to the volume noted for the mouse at the time of treatment initiation (Figure 2*A*).

Immunohistochemistry

For *ex vivo* analysis of tumors, a group of 3 animals per treatment arm were dosed for the first week cycle and were sacrificed following the final MR session. Tumors were harvested and fixed in 10% neutral buffered formalin for a minimum of 48 hours. Tumors were then sectioned and embedded in paraffin followed by cutting sections (5-μm) onto glass slides. Paraffin was removed in xylene, and slides rehydrated using gradually decreasing alcohol concentrations at 2 min/step before ending in tap water (100% ethanol, 95% ethanol, 70% ethanol, water). Slides were then stained using H&E to evaluate cell viability, a Ki-67 antibody to evaluate for cell proliferation and ApopTag to quantify apoptosis after antigen retrieval with Diva (Biocare, Concord, CA) using the Avidin/Biotin Complex System (Vectastain; Vector Labs, Burlingame, CA) and discolored with the DAB solution (Vector Labs).

Capture of images was accomplished for both non-treated and treated brain tumor sections using a digital camera interfaced with an

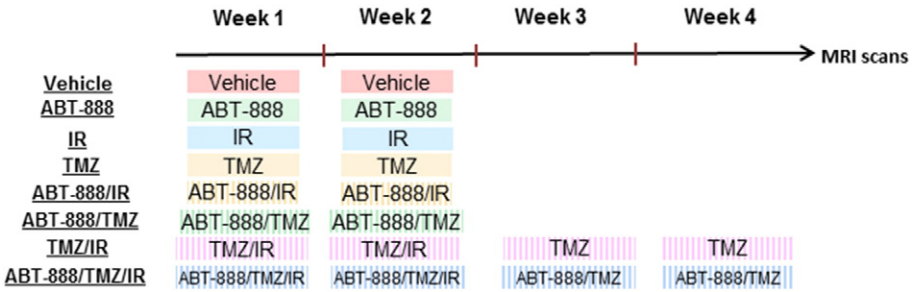

Figure 1. Schematic diagram of treatment schedules. Evaluation of ABT-888, TMZ and IR as monotherapies or combination therapies in a glioblastoma mouse model. Tumor bearing animals were divided into 8 groups and treated with vehicle (1% DMSO in saline), ABT-888 (25 mg/kg per dose, 2 doses a day, 5 d/wk for 2 weeks), TMZ (50 mg/kg per day, 5 d/wk for 2 weeks), IR (1 Gy/day, 5 d/wk for 2 wk), TMZ/ABT-888 (2 weeks of TMZ/ABT-888 treatment), IR/ABT-888 (2 weeks of ABT-888/IR treatment), TMZ/IR (2 weeks of IR/TMZ treatment followed by 2 weeks of TMZ treatment), and TMZ/IR/ABT-888 (2 weeks of IR/TMZ treatment followed by 2 weeks of TMZ/ABT-888 treatment). MRI was used to monitor change in tumor volume every other day.

Olympus microscope. All images were obtained at the same magnification. Because of the heterogeneous nature of the tumors, Ki-67 and apoptosis indices were quantified using the highest staining area. Briefly, staining was checked under low magnification, and then the highest staining area was identified from which images were obtained at 80x magnification. Image analysis was accomplished using ImageJ to quantify Ki-67–positive and ApopTag-positive cells and total cell numbers.

Immunoblotting

Tumor tissue from two individual animals from each of the treatment groups were collected for immunoblotting studies. Tumor tissues were snap-frozen in liquid nitrogen, and stored at −80°C. Tissues were then homogenized in NP-40 lysis buffer supplemented with protease inhibitors and phosphatase inhibitors. Concentration of protein was determined using Lowry assays (Bio-Rad, Hercules, CA). Equal amount of protein were loaded in each lane and resolved by 4% to 12% gradient Bis-Tris gel (Invitrogen, CA). Proteins were transferred to 0.2 μm nitrocellulose membrane (Invitrogen, CA). Membranes were incubated overnight at 4°C with primary antibodies after blocking, followed by incubation with appropriate HRP-conjugated secondary antibody at room temperature for one hour. ECL-Plus was used to detect the activity of peroxidase according to the manufacturer's protocol (Amersham Pharmacia, Sweden). Antibodies raised against PARP-1, pH2A.X(Ser139) were purchased from Cell Signaling Technology (Beverly, MA). Antibody raised against PAR was purchased from Trevigen (Gaithersburg, MD). HRP conjugated beta-actin was purchased from Abcam (Cambridge, MA).

Histological Statistics

Group comparisons of MRI and immunohistologic results were determined at individual time points using analysis of variance and least-squares difference to correct for multiple comparisons. Immunologic differences between groups were assessed using two-tailed Student's *t* test in Prism 6 (GraphPad Software, Inc, La Jolla, CA). All other statistical computations were performed with a statistical software package (SPSS Software Products, Chicago, IL). Statistical significance was assessed at $P < .05$ and all results were presented as means ± SEM.

Imaging Protocols

Groups were followed by MRI to monitor changes in tumor volumes over time for the first three days and then every other day until the conclusion of the study. All *in vivo* MR experiments were performed on a 9.4 Tesla horizontal bore scanner (Agilent Technologies, CA). For MRI examination, mice were anesthetized with isoflurane/air mixture and body temperature was maintained using a heated air system (Air-Therm Heater; World Precision Instruments, FL). MR images of mouse brains were obtained using a two-channel phased array quadrature radio frequency head coil (Rapid Instruments, Germany). Multi-slice axial images were acquired by using a spin echo sequence. T2-weighted images through the brain were produced by using the following parameters: 3 s repetition time, 48 ms echo time, field of view = 20 × 20 mm using a 256 × 128 matrix, slice thickness = 500 μm, number of slices = 25, two signal averages per phase encode step. T1-weighted images were also acquired (TR/TE = 600/17 ms) with similar acquisition parameters as the T2-weighted scans at 10 minutes post-Gd administration (100 μl i.p. of ProHance gadoteridol injection solution) (Bracco Imaging, Germany).

All tumor volumes were quantified using the multi-slice MR images by electronically outlining the tumor boundary visualized on T1 Gd-enhanced images in each slice using image processing software by an individual blinded to the treatment protocol. The number of tumor pixels was converted to an area by multiplication by the factor $[(\text{field of view})^2/(\text{matrix})^2]$. The total tumor volume was calculated as the summed area on all slices. Tumor volumes were averaged within each group and plotted over time.

Diffusion MR scans were used to follow daily changes in tumor cellular density for 5 days posttreatment initiation. Apparent diffusion coefficient (ADC) maps were derived from collected images using a DW spin-echo sequence, equipped with a navigator echo for motion correction and gradient waveforms sensitive to isotropic diffusion, with the following parameters: repetition time/echo time = 4000/37 ms, field of view = 20 × 20 mm^2, matrix size = 128 × 64, slice thickness = 0.5 mm, 25 slices, one average, diffusion time = 40 ms, gradient pulse width = 10 ms, and *b* values (diffusion weighting) = 120 and 1200 s/mm^2. Acquisition time was about 8.5 minutes.

Longitudinal quantification of tumor volumes was accomplished from volumes of interest contoured along the enhancing tumor rim using the contrast-enhanced T1-weighted images. Tumor volumes were used to follow treatment response for the individual treatment groups. The tumor regions were also used to derive whole-tumor means of ADC values over time for individual animals. ADC maps

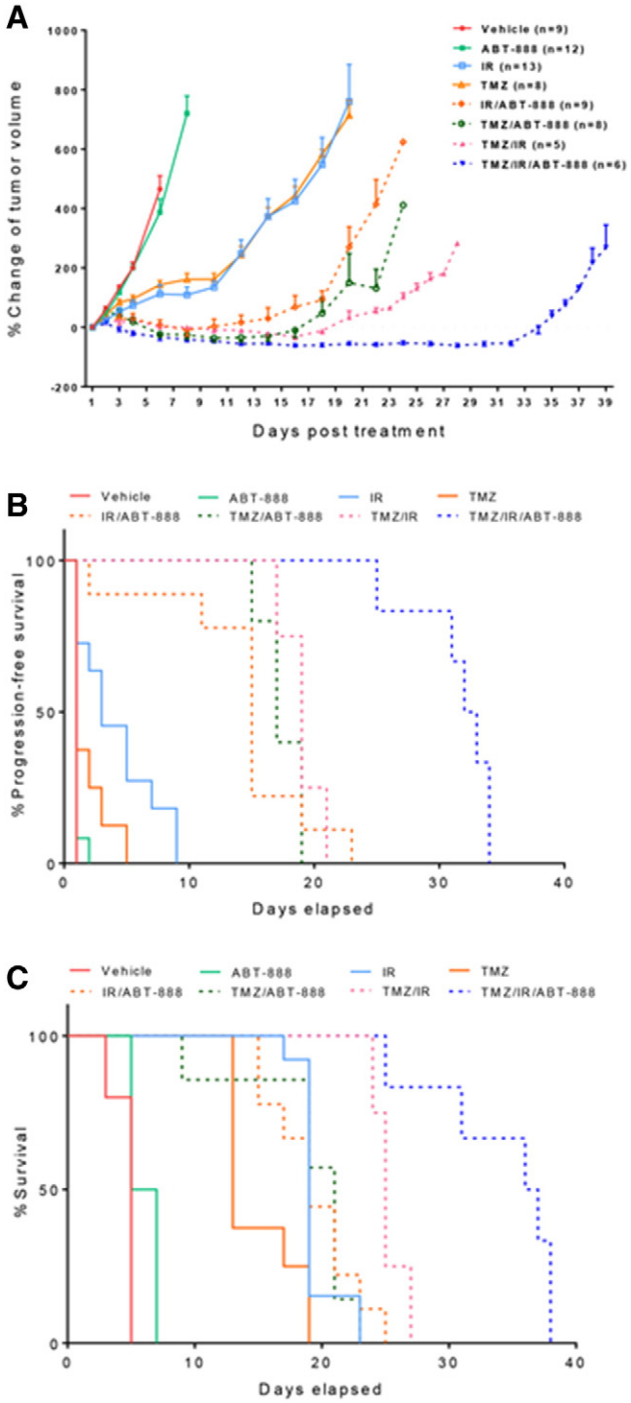

Figure 2. Evaluation of ABT-888, temozolomide (TMZ) and ionizing radiation (IR) as monotherapies or combination therapies in a glioblastoma mouse model. A, Percentage change of intracerebral tumor volumes for vehicle treated control, ABT-888, TMZ, IR, TMZ/ABT-888, IR/ABT-888, TMZ/IR, and TMZ/IR/ABT-888 groups assessed by MRI as a function of time. Note time-to-progression occurred at 20 versus 35 days for TMZ/IR and TMZ/IR/ABT-888 groups, respectively. The graph depicts mean ± SEM. Kaplan-Meier plots for each group are presented for progression-free survival (B) and overall survival (C).

were calculated from the two diffusion weightings (b values) using the following equation:

$$\mathrm{ADC} = \ln(s_1/s_2)/(b_2-b_1),$$

where S_1 and S_2 are the signal intensities at b values b_1 and b_2, respectively, and ADC is the ADC value obtained using b_1 and b_2. Voxels that exhibited insufficient signal, which was defined as <10x noise, in the low b value image (b = 120 s/mm^2) were excluded from the analysis. Response in mean ADC values was assessed by the mean change from baseline to derive a group mean tumor ADC over a day 5 posttreatment initiation time period. Image reconstruction and digital image analysis were done using software algorithms developed in Matlab (The MathWorks, MA).

Data Analysis

Data were presented as mean ± SEM for tumor volume studies. The group comparisons of the percent change in tumor volume were performed at individual time points. Statistical comparisons were made between the control and experimental conditions using the unpaired two-tailed Student's t test. Overall survival and progression-free survival were assessed using a Kaplan-Meier analysis with log-rank test. Statistical significance was assumed at $P < .05$.

Results

Although PTEN deficiency was shown to cause a homologous recombination defect and thus sensitization to PARP inhibitors [27], ABT-888 alone failed to show any anti-tumor effects in this mouse model (Figure 2*A*). Both TMZ and radiation monotherapies delayed did not appear to delay time-to-progression, the treatments did reduce the tumor growth rate by about 7 days as compared with vehicle and ABT-888 groups (Figure 2*A*). Treatment of mice with IR/ABT-888, TMZ/IR and TMZ/ABT-888 had much more pronounced tumor growth delays with time-to-progression of 12, 18 and 20 days, respectively (Figure 2*A*). These results are consistent with previous reports where ABT-888 was effective as a chemosensitization agent in TMZ sensitive tumors [13]. Compared to all other groups, treatment with TMZ/IR/ABT-888 provided the longest time-to-progression (35 days) (Figure 2*A*) and also substantially prolonged progression-free survival and overall survival times over the other treatment groups (Figure 2*B*, $P < .0001$ and Figure 2*C*, $P = .01$). The median survival of the TMZ/IR/ABT-88 group was 36.5 days versus 25 days observed in the TMZ/IR group. A previous study found that concurrent TMZ/IR/ABT-888 showed the trend of extending overall survival in mice, but the overall survival was not significant over TMZ/IR treated mice [13]. Our data showed that concurrent TMZ/IR/ABT-888 with adjuvant TMZ/ABT-888 was more effective than with concurrent TMZ/IR/ABT-888 alone (data not shown).

As concurrent TMZ/IR/ABT-888 with adjuvant TMZ/ABT-888 demonstrated the most significant efficacy in delaying tumor progression among all treatment groups, we compared biological effects to standard-of-care TMZ/IR and ABT-888 alone. PAR western blotting of tumor samples collected three days post treatment initiation are shown in Figure 3. ABT-888 alone greatly reduced the PAR level compared to the vehicle treated group, demonstrating that ABT-888 crossed the blood–brain barrier and was highly effective at suppressing PARP activity. TMZ/IR also decreased PAR level possibly via DNA damage response pathways while TMZ/IR/ABT-888 further reduced PAR to non-detectable levels. Levels of phosphorylation of histone H2Ax, a highly sensitive marker for DNA damage [28] revealed notable DNA damage, as demonstrated by elevated phosphorylated H2Ax levels, occurred in TMZ/IR and TMZ/IR/ABT-888 treated tumors.

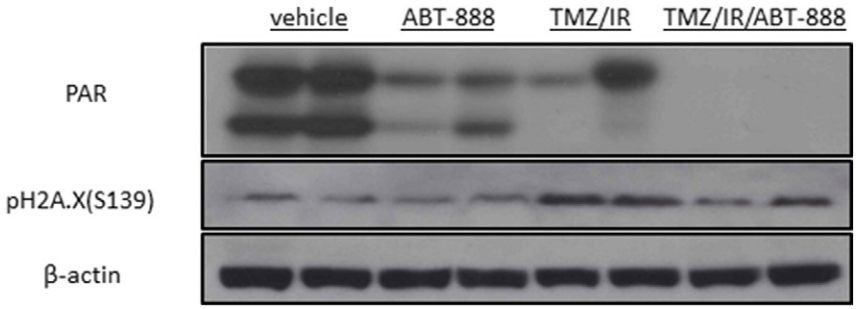

Figure 3. Western blot evaluation of PARP activity and DNA damage in post-treatment tumor tissues. Western blotting using antibodies against PAR, a marker for PARP-1 activity, and pH2Ax, a marker for DNA double strand break. Tumor tissues were harvested from two animals in each group three days post treatment initiation.

To determine the molecular actions of these therapies, whole brain samples underwent IHC evaluation. Induction of apoptosis was compared in each group by the numbers of Apoptag foci. As depicted in Figure 4, *A* and *B*, TMZ/IR/ABT-888 elevated the Apoptag level significantly compared to the other groups demonstrating that TMZ/IR/ABT-888 was most effective in inducing apoptosis. Cell proliferation evaluated by measuring Ki67 levels revealed no significant change for the ABT-888 group compared to vehicle treated group. TMZ/IR reduced Ki67 levels by 43% while TMZ/IR/ABT-888 further reduced Ki67 levels by 70% (Figure 4*A* and B). These data demonstrate that overall TMZ/IR/ABT-888 was a highly efficient combination for inducing apoptosis and reducing cellular proliferation.

In order to facilitate future trials of ABT-888 in clinical practice, we utilized a quantitative imaging biomarker (apparent diffusion coefficient (ADC)) derived from diffusion-weighted MRI scans as it is clinically translatable [18]. Changes in tumor ADC values have been established as a biomarker for monitoring treatment-induced changes in tumor cellular density in GBM [29]. ABT-888 alone did not induce significant change in tumor ADC values (Figure 5, *A* and *B*) which correlated with the trend of increased tumor volumes over time (Figure 1). TMZ/IR/ABT-888 resulted in a rapid increase (10%) in

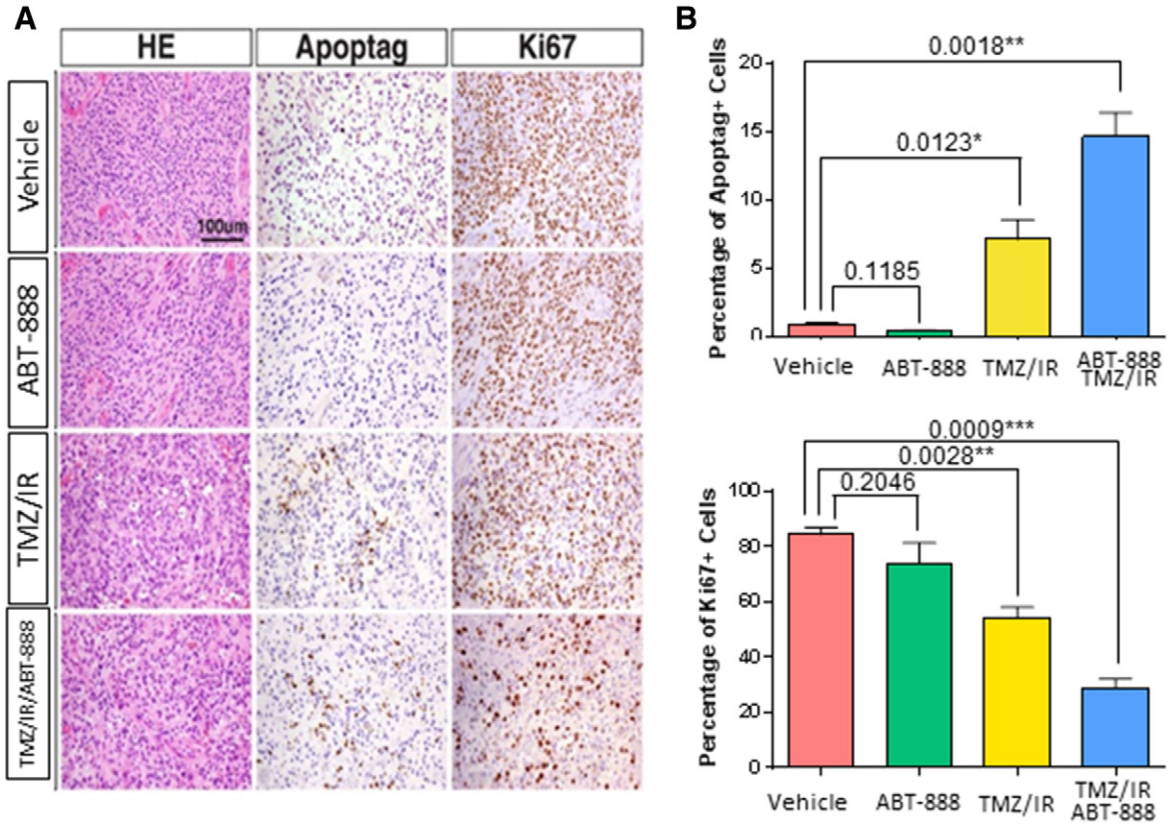

Figure 4. Histopathological analysis of tumor tissue. A, Representative images showing tumor tissue morphology (H&E), apoptosis (Apoptag) and proliferation (Ki67) in tumor tissues from various groups. B, Percentage of apoptotic cells (Apoptag positive) and proliferative cells (Ki67 positive) in each group. The graph depicts mean ± SEM.

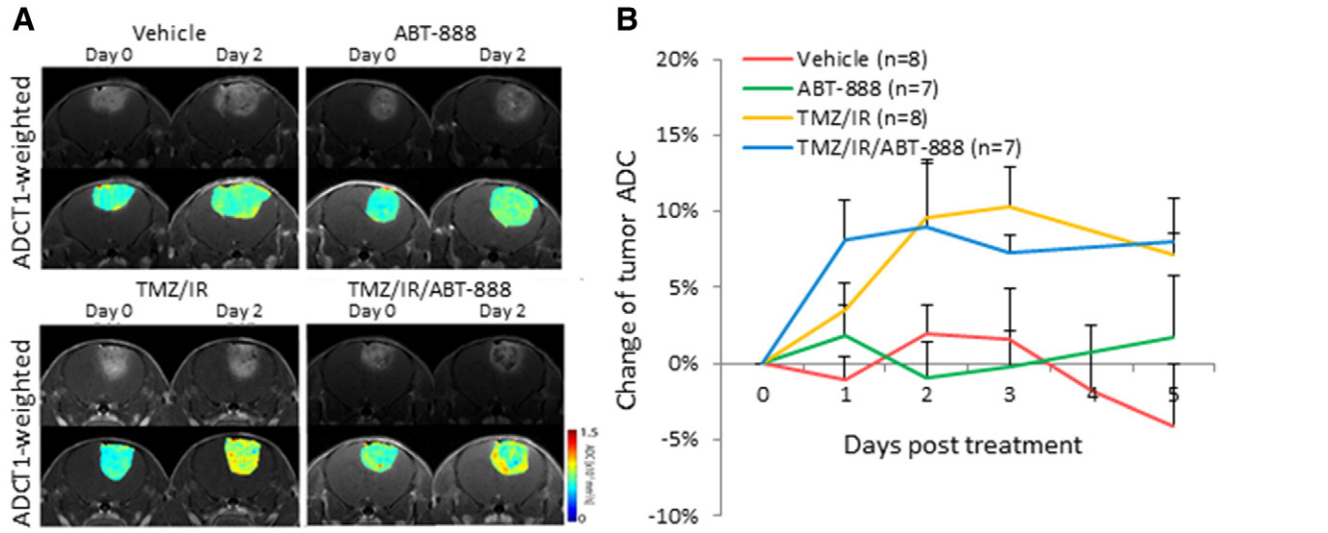

Figure 5. A, Representative T1-weighted and ADC images of various groups prior to treatment initiation and 2 days post treatment initiation. B, Percentage change of mean ADC values for each group. Data is plotted as mean ± SEM.

tumor ADC values, suggesting increased cell death was initiated within 1 day following start of treatment (Figure 5). TMZ/IR also caused elevated ADC values (at 2 days), which also correlated to tumor growth delay at the early stage of treatment (Figure 2*A*).

Discussion

In this study, a GBM genetically engineered mouse model was used to evaluate if administration of a PARP inhibitor would provide additional therapeutic benefit over TMZ/IR therapy. The mouse model was chosen in part due to the fact that it responds to TMZ. It is driven by PDGF that is known to be the initial driver of all gliomas [30]. EGFR is not amplified in the majority of GBM and when it is, it activates the same pathways as PDGF. Thus the model used in this study was an attractive GBM model as generated tumors share high-grade elements such as microvascular proliferation, pseudopalisading necrosis and leaky vasculature with human GBMs. These tumors also closely mimic the proneural subtype of GBM, in which *CDKN2A* (encoding for both *p16INK4A* and *p14ARF*) and *PTEN* deletion are observed in up to 56% and 69% proneural human gliomas, respectively.

We found that in the mouse model used in this study, administration of ABT-888 alone did not have an appreciable effect of tumor growth rate (Figure 2*A*). Both IR and TMZ monotherapies showed overall similar therapeutic response (Figure 2). However, when given in concomitant fashion with either IR (IR/ABT-888) or TMZ (TMZ/ABT-888), additional therapeutic activity was achieved over IR and TMZ monotherapies (Figure 2*A*). It is also interesting to note that both the IR/ABT-888 and TMZ/ABT-888 treatment groups showed similar response to the TMZ/IR treated group in terms of tumor growth delay and progression-free survival (Figure 2). However, the most significant therapeutic response was found in the TMZ/IR/ABT-888 treatment group. Moreover, the TMZ/IR/ABT-888 treated group also had the highest percentage of apoptotic cells and the lowest proliferation signal as measured using Ki67 staining (Figure 4). These results, taken together are very intriguing as clinically, TMZ/IR is given concomitantly followed by adjuvant TMZ thus a GBM clinical trial evaluating addition of a PARP inhibitor along with standard of care (TMZ/IR) appears warranted. Further work may be needed to evaluate if alternative PARP dosage schedules could provide similar therapeutic profiles such as alternating days or weeks, or administration of PARP only post-TMZ/IR thus concomitant with TMZ (TMZ/ABT-888). While the latter suggested dosage schedule may seem reasonable as the combination of TMZ/ABT-888 as an upfront therapy had a significant therapeutic effect (Figure 2*A*) therefore adding it following completion of TMZ/IR may be an alternative strategy. However, in a recently published randomized phase I/II clinical trial it was reported that the combination of TMZ and ABT-888 did not significantly improve 6 month progression-free-survival in recurrent GBM patients who have been previously treated with TMZ [31]. This study also helped to establish dosage and schedules for TMZ and ABT-888 combination therapy which were shown to achieve tolerable levels of treatment adverse events. The NRG oncology ROTG group study [31] along our current results using a mouse GBM, provide an excellent foundation on which to consider including ABT-888 in upfront newly diagnosed GBM. Literature supports the possible use of PARP inhibitors to potentiate TMZ treatment such as in a recent study which showed ABT-888 acted independently to TMZ sensitivity and could override MGMT(–) mediated resistance in serum free cultured glioma GBM cell lines [32]. However, based upon the recent NRG oncology ROTG group study results, it may be assumed that adding ABT-888 to standard of care (TMZ/IR) in newly diagnosed patients may be the most prudent direction to consider assuming a tolerable level of treatment adverse events can be achieved. Thus a trial investigating tolerability and efficacy of concomitant TMZ/IR/ABT-888 followed by adjuvant TMZ/ABT-888 for newly diagnosed GBM should be considered along with DW-MRI as an early quantitative imaging response biomarker.

Optimization of therapeutic strategies can be aided in preclinical and clinical settings through the availability of a biomarker for assessing activity. In this context, we used DW-MRI as an early quantitative imaging response biomarker for these studies as it has been found capable of quantifying early effects of antineoplastic interventions [19,29]. DW-MRI is a sensitive imaging metric capable of detecting and quantifying treatment-associated alterations in microscopic tumor cellular structures which impact water movement

within tissue microenvironment [33]. DW-MRI has been reported useful for early treatment response assessment in glioma patients [18,34,35]. In the present study, we showed that DW-MRI was capable of detecting early increases in tumor ADC values at 1–2 days post-treatment initiation in mice treated with TMZ/IR and TMZ/IR/ABT-888 which persisted over the 5 days in which they were monitored by DW-MRI (Figure 5). The increase in tumor diffusion values indicated that induction of tumor cell death was achieved which correlated with results presented in Figure 4 which revealed an increase in apoptosis in TMZ/IR and TMZ/IR/ABT-888 treatment groups along with an associated decline in proliferation index. Thus, integration of DW-MRI into a clinical GBM trial involving evaluation of a PARP inhibitor such as ABT-888 for monitoring treatment response would provide valuable information for assessing response and could prove useful in providing additional information for real time optimization of dose and schedule.

Conclusions

Results presented reveal that inclusion of ABT-888 in combination with standard of care therapy (TMZ/IR) significantly improved the overall outcome of GBM mice and supports clinical evaluation in this context. DW-MRI was also found useful an image-based biomarker for noninvasive quantification of tumor response. While PARP inhibitors show promise for improving efficacy of TMZ/IR in GBM, optimization of dose and schedule to achieve maximal therapeutic benefit while minimizing hematologic toxicity must be accomplished. Data presented here provides compelling support for continued development of a concurrent TMZ/IR/ABT-888 with adjuvant TMZ/ABT-888 treatment strategy for GBM patients.

Acknowledgements

This work was supported by the National Institutes of Health (P01CA085878 and R35CA197701). Abbott Laboratories provided ABT-888 for this study.

References

[1] Bondy ML, Scheurer ME, Malmer B, Barnholtz-Sloan JS, Davis FG, Il'yasova D, Kruchko C, McCarthy BJ, Rajaraman P, and Schwartzbaum JA, et al (2008). Brain tumor epidemiology: consensus from the Brain Tumor Epidemiology Consortium. *Cancer* **113**, 1953–1968.

[2] Stupp R, Hegi ME, Mason WP, van den Bent MJ, Taphoorn MJ, Janzer RC, Ludwin SK, Allgeier A, Fisher B, and Belanger K, et al (2009). Effects of radiotherapy with concomitant and adjuvant temozolomide versus radiotherapy alone on survival in glioblastoma in a randomised phase III study: 5-year analysis of the EORTC-NCIC trial. *Lancet Oncol* **10**, 459–466.

[3] Curtin NJ (2012). DNA repair dysregulation from cancer driver to therapeutic target. *Nat Rev Cancer* **12**, 801–817.

[4] Bouwman P and Jonkers J (2012). The effects of deregulated DNA damage signalling on cancer chemotherapy response and resistance. *Nat Rev Cancer* **12**, 587–598.

[5] Ame JC, Spenlehauer C, and de Murcia G (2004). The PARP superfamily. *Bioessays* **26**, 882–893.

[6] Barazzuol L, Jena R, Burnet NG, Meira LB, Jeynes JC, Kirkby KJ, and Kirkby NF (2013). Evaluation of poly (ADP-ribose) polymerase inhibitor ABT-888 combined with radiotherapy and temozolomide in glioblastoma. *Radiat Oncol* **8**, 1–11.

[7] Benafif S and Hall M (2015). An update on PARP inhibitors for the treatment of cancer. *Oncotargets Ther* **8**, 519–528.

[8] Sonnenblick A, de Azambuja E, Azim HA, and Piccart M (2015). An update on PARP inhibitors-moving to the adjuvant setting. *Nat Rev Clin Oncol* **12**, 27–41.

[9] Ledermann J, Harter P, Gourley C, Friedlander M, Vergote I, Rustin G, Scott CL, Meier W, Shapira-Frommer R, and Safra T, et al (2014). Olaparib maintenance therapy in patients with platinum-sensitive relapsed serous ovarian cancer: a preplanned retrospective analysis of outcomes by BRCA status in a randomised phase 2 trial. *Lancet Oncol* **15**, 852–861.

[10] Park SR and Chen A (2012). Poly(adenosine diphosphate-ribose) polymerase inhibitors in cancer treatment. *Hematol Oncol* **26**, 649–670.

[11] Albert JM, Cao C, Kim KW, Willey CD, Geng L, Xiao DK, Wang H, Sandler A, Johnson DH, and Colevas AD, et al (2007). Inhibition of poly (ADP-ribose) polymerase enhances cell death and improves tumor growth delay in irradiated lung cancer models. *Clin Cancer Res* **13**, 3033–3042.

[12] Donawho CK, Luo Y, Luo YP, Penning TD, Bauch JL, Bouska JJ, Bontcheva-Diaz VD, Cox BF, DeWeese TL, and Dillehay LE, et al (2007). ABT-888, an orallyactive poly(ADP-ribose) polymerase inhibitor that potentiates DNA-damaging agents in preclinical tumor models. *Clin Cancer Res* **13**, 2728–2737.

[13] Clarke MJ, Mulligan EA, Grogan PT, Mladek AC, Carlson BL, Schroeder MA, Curtin NJ, Lou ZK, Decker PA, and Wu WT, et al (2009). Effective sensitization of temozolomide by ABT-888 is lost with development of temozolomide resistance in glioblastoma xenograft lines. *Mol Cancer Ther* **8**, 407–414.

[14] Gupta SK, Mladek AC, Carlson BL, Boakye-Agyeman F, Bakken KK, Kizilbash SH, Schroeder MA, Reid J, and Sarkaria JN (2014). Discordant in vitro and in vivo chemopotentiating effects of the PARP inhibitor veliparib in temozolomide-sensitive versus -resistant glioblastoma multiforme Xenografts. *Clin Cancer Res* **20**, 3730–3741.

[15] Palma JP, Wang YC, Rodriguez LE, Montgomery D, Ellis PA, Bukofzer G, Niquette A, Liu XS, Shi Y, and Lasko L, et al (2009). ABT-888 confers broad in vivo activity in combination with temozolomide in diverse tumors. *Clin Cancer Res* **15**, 7277–7290.

[16] Reiss KA, Herman JM, Zahurak M, Brade A, Dawson LA, Scardina A, Joffe C, Petito E, Hacker-Prietz A, and Kinders RJ, et al (2015). A Phase I study of veliparib (ABT-888) in combination with low-dose fractionated whole abdominal radiation therapy in patients with advanced solid malignancies and peritoneal carcinomatosis. *Clin Cancer Res* **21**, 68–76.

[17] Su JM, Thompson P, Adesina A, Li XN, Kilburn L, Onar-Thomas A, Kocak M, Chyla B, McKeegan E, and Warren KE, et al (2014). A phase I trial of veliparib (ABT-888) and temozolomide in children with recurrent CNS tumors: a Pediatric Brain Tumor Consortium report. *Neuro-Oncology* **16**, 1661–1668.

[18] Chenevert TL, Stegman LD, Taylor JM, Robertson PL, Greenberg HS, Rehemtulla A, and Ross BD (2000). Diffusion magnetic resonance imaging: an early surrogate marker of therapeutic efficacy in brain tumors. *J Natl Cancer Inst* **92**, 2029–2036.

[19] Padhani AR, Liu G, Koh DM, Chenevert TL, Thoeny HC, Takahara T, Dzik-Jurasz A, Ross BD, Van Cauteren M, and Collins D, et al (2009). Diffusion-weighted magnetic resonance imaging as a cancer biomarker: consensus and recommendations. *Neoplasia* **11**, 102–125.

[20] Hambardzumyan D, Amankulor NM, Helmy KY, Becher OJ, and Holland EC (2009). Modeling adult gliomas using RCAS/t-va technology. *Transl Oncol* **2**, 89–95.

[21] Dai C, Celestino JC, Okada Y, Louis DN, Fuller GN, and Holland EC (2001). PDGF autocrine stimulation dedifferentiates cultured astrocytes and induces oligodendrogliomas and oligoastrocytomas from neural progenitors and astrocytes in vivo. *Genes Dev* **15**, 1913–1925.

[22] Koutcher JA, Hu XY, Xu S, Gade TPF, Leeds N, Zhou XHJ, Zagzag D, and Holland EC (2002). MRI of mouse models for gliomas shows similarities to humans and can be used to identify mice for preclinical trials. *Neoplasia* **4**, 480–485.

[23] McConville P, Hambardzumyan D, Moody JB, Leopold WR, Kreger AR, Woolliscroft MJ, Rehemtulla A, Ross BD, and Holland EC (2007). Magnetic resonance imaging determination of tumor grade and early response to temozolomide in a genetically engineered mouse model of glioma. *Clin Cancer Res* **13**, 2897–2904.

[24] Pitter KL, Galban CJ, Galban S, Saeed-Tehrani O, Li F, Charles N, Bradbury MS, Becher OJ, Chenevert TL, and Rehemtulla A, et al (2011). Perifosine and CCI 779 co-operate to induce cell death and decrease proliferation in PTEN-intact and PTEN-deficient PDGF-driven murine glioblastoma. *PLoS One* **6**.

[25] Tchougounova E, Kastemar M, Brasater D, Holland EC, Westermark B, and Uhrbom L (2007). Loss of Arf causes tumor progression of PDGFB-induced oligodendroglioma. *Oncogene* **26**, 6289–6296.

[26] Verhaak RG, Hoadley KA, Purdom E, Wang V, Qi Y, Wilkerson MD, Miller CR, Ding L, Golub T, and Mesirov JP, et al (2010). Integrated genomic analysis identifies clinically relevant subtypes of glioblastoma characterized by abnormalities in PDGFRA, IDH1, EGFR, and NF1. *Cancer Cell* **17**, 98–110.

[27] Mendes-Pereira AM, Martin SA, Brough R, McCarthy A, Taylor JR, Kim JS, Waldman T, Lord CJ, and Ashworth A (2009). Synthetic lethal targeting of PTEN mutant cells with PARP inhibitors. *EMBO Mol Med* **1**, 315–322.

[28] Rogakou EP, Pilch DR, Orr AH, Ivanova VS, and Bonner WM (1998). DNA double-stranded breaks induce histone H2AX phosphorylation on serine 139. *J Biol Chem* **273**, 5858–5868.

[29] Thoeny HC and Ross BD (2010). Predicting and monitoring cancer treatment response with diffusion-weighted MRI. *J Magn Reson Imaging* **32**, 2–16.

[30] Ozawa T, Riester M, Cheng YK, Huse JT, Squatrito M, Helmy K, Charles N, Michor F, and Holland EC (2014). Most human non-GCIMP glioblastoma subtypes evolve from a common proneural-like precursor glioma. *Cancer Cell* **26**, 288–300.

[31] Robins HI, Zhang P, Gilbert MR, Chakravarti A, de Groot JF, Grimm SA, Wang F, Lieberman FS, Krauze A, and Trotti AM, et al (2015). A randomized phase I/II study of ABT-888 in combination with temozolomide in recurrent temozolomide resistant glioblastoma: an NRG oncology RTOG group study. *J Neuro-Oncol* [Epub ahead of print] PMID: 26508094.

[32] Balvers RK, Lamfers ML, Kloezeman JJ, Kleijn A, Berghauser Pont LM, Dirven CM, and Leenstra S (2015). ABT-888 enhances cytotoxic effects of temozolomide independent of MGMT status in serum free cultured glioma cells. *J Transl Med* **13**, 74.

[33] Rowley HA, Grant PE, and Roberts TP (1999). Diffusion MR imaging. Theory and applications. *Neuroimaging Clin N Am* **9**, 343–361.

[34] Ellingson BM, Malkin MG, Rand SD, Connelly JM, Quinsey C, LaViolette PS, Bedekar DP, and Schmainda KM (2010). Validation of functional diffusion maps (fDMs) as a biomarker for human glioma cellularity. *J Magn Reson Imaging* **31**, 538–548.

[35] Hamstra DA, Chenevert TL, Moffat BA, Johnson TD, Meyer CR, Mukherji SK, Quint DJ, Gebarski SS, Fan X, and Tsien CI, et al (2005). Evaluation of the functional diffusion map as an early biomarker of time-to-progression and overall survival in high-grade glioma. *Proc Natl Acad Sci U S A* **102**, 16759–16764.